Dispersion-Free Solvent Extraction with Microporous Hollow-Fiber Modules

Extensive studies on dispersion-free solvent extraction have been carried out using modules made with either hydrophobic or hydrophilic microporous hollow-fiber membranes. Membrane and boundary layer resistances have been characterized for both kinds of hollow fiber using solvent extraction systems with a wide variation of distribution coefficients and interfacial tensions. It has been found that the Graetz solution for a constant wall concentration describes satisfactorily mass transfer on the lumen side of a hollow-fiber device. A correlation of the form $N_{Sh} = [D_h(1 - \phi)/L]N_{Re}^{0.6}N_{Sc}^{0.33}$ appears to provide a close fit to the shell-side mass transfer coefficient data. The performance characteristics of dispersion-free extraction in hollow-fiber modules have been considered against those of commercial packed-bed extractors. A perspective has been provided on comparative utilities of hydrophobic or hydrophilic hollow fibers for a given solvent extraction problem.

R. Prasad, K. K. Sirkar
Department of Chemistry and
Chemical Engineering
Stevens Institute of Technology
Hoboken, NJ 07030

Introduction

Dispersion-free contacting of immiscible phase pairs using microporous membranes is being explored increasingly for equilibrium separation of liquid solutions or gaseous mixtures. Consider recent studies in dispersion-free solvent extraction using flat microporous hydrophobic membranes (Kiani et al., 1984; Prasad et al., 1986) and flat microporous hydrophilic and composite hydrophilic-hydrophobic membranes (Prasad and Sirkar, 1987a,b). Such a technique with microporous hollow fibers (MHF) may provide high mass transfer rates per unit volume since hollow-fiber modules can pack an enormous surface area (Kiani et al., 1984). The technique also overcomes other shortcomings of conventional liquid extraction such as flooding limitations on independent variation of phase flow rates, requirement of density difference, and inability to handle particulates. Recent studies on nondispersive gas absorption (Qi and Cussler, 1985; Yang and Cussler, 1986; Radovich et al., 1986) using microporous hydrophobic hollow-fiber modules illustrate their considerable potential.

Frank and Sirkar (1985, 1986) have demonstrated dispersion-free solvent extraction using hydrophobic hollow fibers with solvent flow through the fiber lumen and an aqueous fermentation broth on the shell side containing immobilized biocatalyst particles. They have achieved O_2 supply and CO_2 removal through the MHF bore as alcohol production proceeded on the shell side (a three-phase trickle-bed reactor). Although Prasad and Sirkar (1987a) have studied solvent extraction with hydrophobic MHF, it was very limited in nature. Their prime focus was on solvent extraction with flat microporous membranes in its various ramifications. Dahuron and Cussler (1987) have recently presented MHF solvent extraction data for bioproducts purification with aqueous biphasic and reverse micelle systems. A comprehensive investigation of dispersion-free solvent extraction with hollow-fiber modules is not available. In this paper, we have therefore undertaken such a study.

We have experimentally investigated the contributions of the two liquid-phase mass transfer coefficients and the membrane mass transfer coefficient to the overall solute transfer coefficient in MHF modules containing either hydrophobic or hydrophilic hollow fibers. The role of the solute distribution coefficient, m_i, in the above relationships has been studied using the following solvent-water-solute systems with m_i values varying between 118 and 0.013:

Methyl isobutyl ketone (MIBK)-water-phenol ($m_i \sim 118$)
n-Butanol–water–succinic acid ($m_i \sim 1.5$)
MIBK-water-acetic acid ($m_i \sim 0.5$)
Xylene-water-acetic acid ($m_i \sim 0.013$)

These systems provided also a spectrum of interfacial tensions.

Membrane transport resistances of two kinds of hollow fibers for the different systems have been isolated. Applicability of the notion of unhindered solute diffusion through tortuous mem-

Correspondence concerning this paper should be addressed to K. K. Sirkar.

brane pores containing either an aqueous solution or an organic solvent has been investigated. The mass transfer coefficient for each bulk liquid phase has been determined and its functional dependences have been identified *vis-a-vis* known mass transfer correlations. The mechanism of hollow-fiber function in achieving the observed solute extraction rates has been illustrated with modules having as high a hollow-fiber surface area per unit contactor volume a as 4,684 m^2/m^3. Solvent extraction capabilities of a hydrophobic hollow-fiber module have been compared with those of a hydrophilic hollow-fiber module and conventional dispersion-based extractors. The analysis and correlations of this study allow rational steps to be taken toward the design of MHF extractors for systems without any chemical reaction.

Theoretical Basis for Experimental Measurement Strategies

Previous studies with small flat membranes have shown that the overall mass transfer resistance to solute transport in dispersion-free extraction could be adequately described by the conventional procedure of adding the various resistances (Kiani et al., 1984; Prasad et al., 1986; Prasad and Sirkar, 1987a, b). Thus, at any axial location in a hollow-fiber module such an additivity of resistance relation is likely to be valid. Since we have two kinds of MHF modules, hydrophobic and hydrophilic, and the fiber lumen may have either organic or aqueous phase, four different configurations, shown in Figure 1, are possible. In all cases, hydrophobic membrane pores are assumed to be filled with the organic phase while hydrophilic membrane pores contain the aqueous phase.

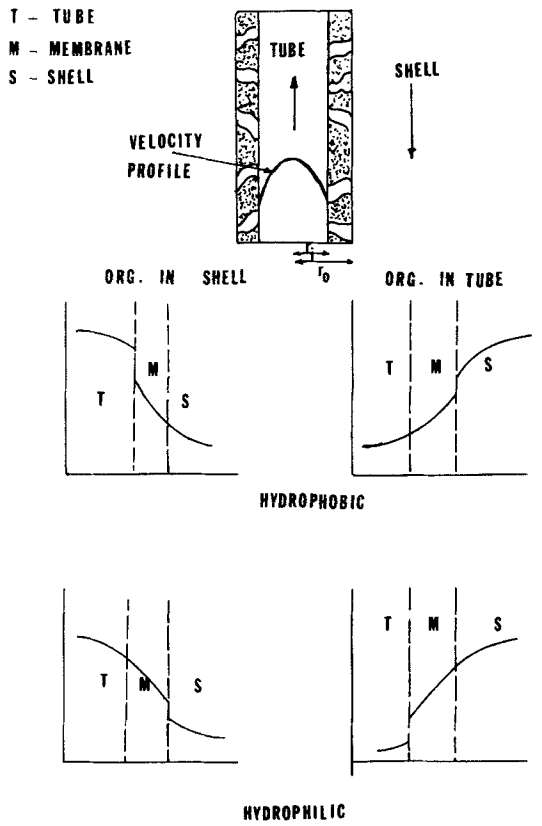

Figure 1. Concentration profiles for hydrophilic and hydrophobic MHF.

The following four relations are relevant to our analysis of an overall mass transfer coefficient K_o based on organic phase:

Hydrophobic MHF

Organic on lumen (tube) side

$$1/K_o d_o = 1/k_{ot} d_i + 1/k_{mo} d_{lm} + m_i/k_{ws} d_o \tag{1}$$

Organic on shell side

$$1/K_o d_i = 1/k_{os} d_o + 1/k_{mo} d_{lm} + m_i/k_{wt} d_i \tag{2}$$

Hydrophilic MHF

Organic on lumen (tube) side

$$1/K_o d_i = 1/k_{ot} d_i + m_i/k_{mw} d_{lm} + m_i/k_{ws} d_o \tag{3}$$

Organic on shell side

$$1/K_o d_o = 1/k_{os} d_o + m_i/k_{mw} d_{lm} + m_i/k_{wt} d_i \tag{4}$$

For systems with $m_i \gg 1$, the following alternative formulations utilizing an overall mass transfer coefficient K_w based on aqueous phase are more useful:

Hydrophobic MHF

Aqueous flow on shell side

$$1/K_w d_o = 1/k_{ws} d_o + 1/m_i k_{mo} d_{lm} + 1/m_i k_{ot} d_i \tag{5}$$

Aqueous flow on tube side

$$1/K_w d_i = 1/k_{wt} d_i + 1/m_i k_{mo} d_{lm} + 1/m_i k_{os} d_o \tag{6}$$

Hydrophilic MHF

Aqueous flow on tube side

$$1/K_w d_o = 1/k_{wt} d_i + 1/k_{mw} d_{lm} + 1/m_i k_{os} d_o \tag{7}$$

Aqueous flow on shell side

$$1/K_w d_i = 1/k_{ws} d_o + 1/k_{mw} d_{lm} + 1/m_i k_{ot} d_i \tag{8}$$

In all these relations, the overall mass transfer coefficient is defined with respect to the hollow-fiber surface area where the interface of the immiscible aqueous-organic phases is located.

The membrane mass transfer coefficient is most likely to be independent of aqueous or organic flow rates. However the tube-side mass transfer coefficient will vary with $v_{aq}^{\nu_t}$ or $v_{or}^{\nu_t}$ depending on whether aqueous or organic phase flows on the tube side. Similarly, the shell-side mass transfer coefficient will vary with $v_{aq}^{\nu_s}$ or $v_{or}^{\nu_s}$ depending on whether the aqueous or organic phase flows on the shell side. The values of ν_t or ν_s will be different from each other and will have to be determined by regression analysis of K_o or K_w and v_{or} or v_{aq} data.

Relations 1–8 are valid at any axial location of the MHF extractor. The values of K_o or K_w measured experimentally are based on the whole extractor module using a logarithmic mean concentration difference and are identified as $\bar{K}_o$ or $\bar{K}_w$. If we assume for the purpose of a first-order analysis that such module-averaged overall solute transfer coefficients are related to

module-averaged $\bar{k}_o$ and $\bar{k}_w$ by the same relations, Eqs. 1–8, then considerable progress can be made by analyzing the behavior of the MHF modules under some limiting conditions of m_i.

To predict $\bar{K}_o$ or $\bar{K}_w$ for any system, one needs to know $\bar{k}_{ws}$ or $\bar{k}_{wt}$, $\bar{k}_{os}$ or $\bar{k}_{ot}$, and k_{mw} or k_{mo}. The strategy is to isolate each of these quantities by choosing proper experimental conditions, explore how the boundary layer coefficients vary with the dimensionless numbers (N_{Re} and N_{Sc}), and if possible, quantify mass transfer correlations for the shell and lumen sides of the MHF modules. An inherent assumption in the following analysis is that the tube-side, shell-side, and membrane mass transfer coefficients are of the same order of magnitude.

Case 1: $\mathbf{m_i \ll 1}$

Hydrophobic MHF. The organic film transfer coefficient $\bar{k}_{ot}$ or $\bar{k}_{os}$ will vary with $v_{or}^{\nu_t}$ or $v_{or}^{\nu_s}$ depending on whether the organic flow is on the tube side or the shell side. Plotting $1/\bar{K}_o$ against $(v_{or})^{-\nu_t}$ or $(v_{or})^{-\nu_s}$ will lead essentially to a value of zero for $1/\bar{k}_{ot}$ or $1/\bar{k}_{os}$ in the limit $(v_{or})^{-\nu}$ tending to zero (by the Wilson-plot technique [Wilson, 1915]). From Eqs. 1 and 2, the intercept on the $1/\bar{K}_o$ axis will then be a function of $1/k_{mo}$ only. From this intercept, the value of k_{mo} can be found. By subtracting the value of this intercept from the $1/\bar{K}_o$ at various v_{or}, the values of $\bar{k}_{ot}$ or $\bar{k}_{os}$ can be found as a function of v_{or} on the tube or shell side.

Hydrophilic MHF. Analysis similar to that above will now yield an intercept of zero on the $1/\bar{K}_o$ axis for organic flow on both shell and tube sides of the MHF module, Eqs. 3 and 4. The magnitudes of $\bar{K}_o$ at different v_{or}-s are numerically equal to the values of $\bar{k}_{os}$ or $\bar{k}_{ot}$ at the same v_{or}-s. The values of $\bar{k}_{ot}$ and $\bar{k}_{os}$ obtained here as well as from hydrophobic membrane modules can be used to develop correlations for the tube- and shell-side mass transfer coefficients.

Case 2: $\mathbf{m_i \gg 1}$

Hydrophobic MHF. The situation here is similar to that of the hydrophilic MHF for $m_i \ll 1$. The plot of $1/\bar{K}_w$ against $(v_{aq})^{-\nu_t}$ or $(v_{aq})^{-\nu_s}$ will yield an intercept of zero on the $1/\bar{K}_w$ axis, Eqs. 5 and 6. The numerical value of $\bar{K}_w$ at any v_{aq} will be that of $\bar{k}_{ws}$ or $\bar{k}_{wt}$.

Hydrophilic MHF. As in the case of the hydrophobic MHF with $m_i \ll 1$, the intercept on $1/\bar{K}_w$ axis in plots of $1/\bar{K}_w$ vs. $(v_{wt})^{-\nu_t}$ or $(v_{ws})^{-\nu_s}$ will be a function of k_{mw} only, Eqs. 7 and 8. This value of the intercept can be subtracted from the $1/\bar{K}_w$ values at different v_{aq} to yield the values of $\bar{k}_{wt}$ or $\bar{k}_{ws}$ as functions of v_{aq}. Again, these values together with values obtained earlier, can be utilized to develop correlations for the shell- and tube-side mass transfer coefficients.

Case 3: $\mathbf{m_i \simeq 1}$

Hydrophobic MHF. The full Eqs. 1 and 2 are applicable for $m_i \sim 1$. The Wilson-plot technique will yield an intercept that will be related to the membrane mass transfer resistance ($1/k_{mo}$) by the following relations:

$$1/\bar{K}_o d_o|_{\text{intercept}} = 1/k_{mo} d_{lm} + m_i/\bar{k}_{ws} d_o \quad \text{(organic, tube side)} \quad (9)$$

$$1/\bar{K}_o d_i|_{\text{intercept}} = 1/k_{mo} d_{lm} + m_i/\bar{k}_{wt} d_i \quad \text{(organic, shell side)} \quad (10)$$

The values of $\bar{k}_{ws}$ and $\bar{k}_{wt}$ can be calculated from the correlations developed earlier. Hence the membrane resistance k_{mo} can be estimated. The values of these above intercepts, when subtracted from the values of $1/\bar{K}_o$ of the $1/\bar{K}_o$ vs. v_{or}^{ν} data, will yield $\bar{k}_{os}$ or $\bar{k}_{ot}$ vs. v_{or} data. These organic film coefficients can now be used in addition for the development of correlations for tube- and shell-side mass transfer coefficients.

Hydrophilic MHF. The full Eqs. 3 and 4 have to be used and will now yield intercepts that are functions of both $\bar{k}_w$ and k_{mw}. If $\bar{k}_{ws}$ and $\bar{k}_{wt}$ are again estimated by using correlations developed earlier, the membrane resistance k_{mw} can be found for both organic flow on the shell side and organic flow on the tube side. These intercept values can then be subtracted from the measured $\bar{K}_o$ values obtained to get $\bar{k}_{ot}$ and $\bar{k}_{os}$ as functions of v_{or} on the shell and tube sides; hence correlations can be developed for the film transfer coefficients.

The above procedures can be used to obtain the tube- and shell-side film transfer coefficients for a variety of solvent extraction systems with a wide variation of m_i, N_{Sc}, and N_{Re}. All the above data can now be utilized to develop correlations for the dimensionless tube- and shell-side Sherwood number N_{Sh}.

Membrane mass transfer coefficient

The experimentally obtained membrane resistances $1/k_{mo}$ and $1/k_{mw}$ may be described on the basis of earlier flat-membrane studies by

$$k_{mo} = D_{io}\epsilon_M/[\tau_M(d_o - d_i)/2];$$
$$k_{mw} = D_{iw}\epsilon_M/[\tau_M(d_o - d_i)/2] \quad (11)$$

if unhindered diffusion takes place through the liquid filling the tortuous pores of the membrane. The value of the tortuosity factor τ_M obtained for a given membrane for the different solvent extraction systems should be the same unless the assumption of hindered diffusion breaks down, all other porous membrane characteristics remaining constant.

Experimental Method

Chemicals and materials

The following chemicals were used in this study:

1. Xylene (certified ACS grade, Fischer Scientific, Fairlawn, NJ)
2. MIBK (certified ACS grade, Fischer Scientific)
3. Acetic acid (glacial reagent, ACS grade, Fischer Scientific)
4. Isopropyl alcohol (IPA) (HPLC grade, Fischer Scientific)
5. Methanol (HPLC grade, Fischer Scientific)
6. Acetonitrile (HPLC grade, Fischer Scientific)
7. Succinic acid (purified crystals, Merck and Co., Rahway, NJ)
8. Sodium hydroxide (NaOH) (certified ACS grade, Fischer Scientific)
9. *n*-Butanol (analytical reagent, Mallinckrodt, Paris, KY)
10. Oxalic acid (anhydrous analytical grade, Coleman and Bell, Norwood, OH)
11. Phenol (loose crystals, Coleman and Bell)

Table 1 shows the physical properties of the microporous hollow-fiber membranes used in this study. These membranes were

Table 1. Physical Properties* of Hollow-fiber Membranes Used

Membrane	Material	Pore Size μm	OD μm	ID μm	Porosity
Celgard X-20	Polypropylene	0.03	290	240	0.4
Cuprophan C1-1M-11/200	Regenerated cellulose	**	200†	140†	0.55†

*From manufacturer's catalog
**Pore size not available in manufacturer's catalog
†Measured in our laboratory

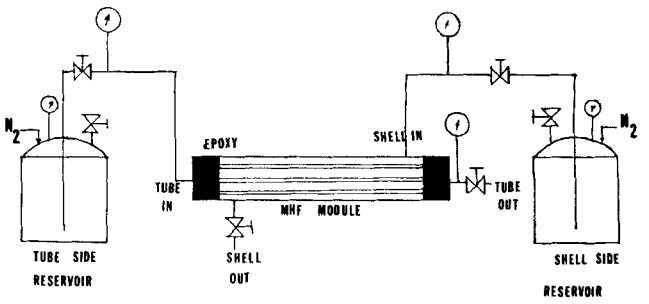

Figure 2. Flow loop for solvent extraction studies and diagram of a MHF module.

obtained as follows:

Polypropylene hollow fibers (X-20 from Celanese Separations Products, Charlotte, NC)

Regenerated cellulose hollow fibers (CUPROPHAN type C1-1M-11/200 from ENKA, FRG)

CUPROPHAN hollow fibers are supplied with a nonvolatile solvent in the pores and the bore of the membrane to prevent pore collapse. Before use for solvent extraction studies, the nonvolatile solvent was leached out using IPA. The membranes were soaked in IPA with gentle stirring for 3 h and then dried in air at room temperature overnight (12 h).

A diagram of a hollow-fiber module is shown in Figure 2. These modules resembled a shell-and-tube heat exchanger with the tube sheets made of a solvent resistant epoxy. The shell of these modules consisted of a 6.25 mm stainless steel tubing with a 6.25 mm male run tee at either end. Internal threads were tapped in the run tees to provide good adhesion of the epoxy with the fitting. The epoxy selected was a two-component system of Armstrong C-4 epoxy with "D" activator (Beacon Chemicals, Mt. Vernon, NY) mixed in an epoxy:activator ratio of 4:1. The MHF modules were made with careful control over the uniform spreading of the epoxy over the fibers and subsequent curing of the epoxy. The details are available in a thesis by Prasad (1986). The full cure strength of the epoxy was achieved at the end of a week.

The first hydrophobic MHF module was made by potting the hydrophobic X-20 hollow fibers in a 12.5 mm dia. stainless steel nipple. The shell-side fluid inlet and outlet ports were constructed by drilling 6.25 mm holes in the shell at appropriate points and tapping female NPT threads in the holes. This module could not be used at over 13.4×10^4 N/m^2 shell-side pressure due to leaks at the shell-side ports. Further details of other MHF modules are given in Table 2.

Organic acid concentrations in the organic and aqueous phases were determined by titration against standardized NaOH solution. The procedure followed is essentially the same as that outlined in Kiani et al. (1984). Phenol concentration measurements utilized a HP 1090 LC with a 100 × 4.6 mm Hypersil ODS 5 μm reverse-phase column and a UV detector set at 254 nm. The mobile phase was acetonitrile-water with gradient elution (the mobile phase concentration changing from 100% water to 40% acetonitrile–60% water in 7 min at a flow rate of 4 cm^3/min).

Determination of membrane parameters

Hydrophilic membranes of regenerated cellulose swell in contact with aqueous solution. This swelling is three-dimensional in nature and affects the pore size, thickness, and porosity of the membrane. Thickness and porosity of these membranes are hence to be determined in contact with aqueous solutions used in this study. This was done by first soaking a single hollow fiber in the aqueous feed solution and then examining the fiber under a microscope (Zeiss, FRG) using polarized light. The fiber OD and ID can thus be measured under wet conditions. The wet weight of the hollow fiber is next found, then the fiber dried in an oven at 100°C for 12 h and the dry weight of the fiber noted. The porosity of the membrane is found from the above weighings and the following relation:

$$\text{Porosity} = \text{pore vol.}/(\text{pore vol.} + \text{vol. of cellulose}) \quad (12)$$

Table 2. Hollow-fiber Module Details

Membrane	Module No.	Shell	No. of Fibers	Length cm	Shell-side Void Frac.	a cm^{-1}
Celgard X-20	1	12.5 mm S.S. pipe	114	15.8	0.96	5.3
Celgard X-20	2	6.25 mm S.S. tube	54	16.0	0.803	27.2
Celgard X-20	3	6.25 mm S.S. tube	102	16.0	0.6	46.84
Cuprophan	1	6.25 mm S.S. tube	50	18	0.913	17.36
Cuprophan	2	6.25 mm S.S. tube	50	6.0	0.913	18.0

where

Pore vol = (wet membrane wt.

$$- \text{dry membrane wt.})/\text{solution density} \quad (13)$$

and

Wet membrane wt. = wt. measured

$$- (\pi/4)\, d_i^2 L \times \text{solution density} \quad (14)$$

The density of cellulose was taken as 1.52 g/cm^3 (Malm et al., 1974). The reproducibility of the wet and dry membrane weights was within 5%.

The tortuosity of the hydrophilic hollow fiber was also found by gas permeation across the aqueous solution immobilized in the pores of the membrane in the manner of Bhave and Sirkar (1986a, b). Further details of the measurements are available in Prasad (1986) as well as in Prasad and Sirkar (1987b).

Procedures

The flow loop for the MHF test system is shown schematically in Figure 2. The hydrophobic membrane modules were operated with the aqueous phase at a higher pressure than the organic phase pressure. Experiments were done with the aqueous phase flow on the tube side (organic flow on the shell side) as well as with the aqueous flow on the shell side (organic flow on tube side). Care was taken to ensure that the aqueous phase pressure was greater than the organic phase pressure at every location in the permeator. In the case of hydrophilic MHF modules, the solvent (organic) phase was always kept at a pressure higher than the aqueous phase pressure. Again, experiments were done with the organic phase on the shell side (aqueous phase on tube side) as well as with organic phase on tube side (aqueous phase on shell side).

The overall mass transfer coefficient was calculated using the following relation

$$Q_{or} C_{io}^b|_{exit} = \bar{K}_o \times \Delta C|_{LM} \times \text{area of contact} \quad (15)$$

where

$$\Delta C|_{LM} = (\Delta C_1 - \Delta C_2)/ln(\Delta C_1/\Delta C_2) \quad (15a)$$

$$\Delta C_1 = m_i C_{iw}^b|_{in} - C_{io}^b|_{out} \quad (15b)$$

$$\Delta C_2 = m_i C_{iw}^b|_{out} \quad (15c)$$

and the area of contact is based on d_i or d_o, depending on where the aqueous-organic interface is located.

Overall mass transfer coefficient based on aqueous phase $\bar{K}_w$ was found by relation 15 where ΔC's are now defined as

$$\Delta C_1 = C_{iw}^b|_{in} - C_{io}^b/m_i \quad (15d)$$

$$\Delta C_2 = C_{iw}^b|_{out} \quad (15e)$$

It should be noted that for a high-m_i once-through system where not much solute is extracted into the organic phase, ΔC_1, defined by Eq. 15d, will be approximately equal to the inlet concentration of the aqueous feed.

The membrane tortuosities were calculated using Eq. 11, where k_{mo} or k_{mw} was determined from experimental data, D_{io} or D_{iw} is given in Table 3, and d_i, d_o, and ϵ_M are known for the fibers.

Results

The results of the distribution coefficient measurements for the different extraction systems used here are shown in Table 3. The values of m_i remain essentially constant in the concentration ranges used in this work. Values of m_i from other literature references are also shown. The results of overall mass transfer coefficient measurements are presented and analyzed next.

Hydrophobic MHF

Wilson plots of $1/\bar{K}_o$ vs. $v_{or}^{-\nu}$ are shown in Figures 3 and 4. The same figures also show the plots of $1/\bar{K}_w$ vs. $v_{aq}^{-\nu}$ for the high-m_i system (MIBK-water-phenol). The value of the exponent ν was

Table 3. Distribution and Diffusion Coefficients of Solutes*

Liquid Extrac. System (Solvent-Feed-Solute)	$D_{io} \times 10^5$ cm^2/s	$D_{iw} \times 10^5$ cm^2/s	$C_{iw}^b \times 10^3$ mol/cm^3	m_i	m_i Lit. Values
Xylene-water-acetic acid	2.76	—	4.75	0.039	—
	2.76	—	2.33	0.025	—
	2.76	—	0.96	0.0125	—
	2.76	—	0.42	0.0125	—
	2.76	—	0.27	0.013	—
MIBK-Water-acetic-acid	3.2	1.24	4.15	0.5103	—
	3.2	1.24	1.8	0.532	0.54
	3.2	1.24	0.42	0.523	(a)
n-Butanol–water–succinic acid	0.3	0.54	0.92	1.48	1.3
	(a)	(a)	0.44	1.50	(a)
MIBK-water-phenol (pH 6.8)	—	0.99	0.0026	118	108
	—	—	0.0015	120	—
	—	—	0.26	—	50 (b)

*Diffusion coefficients estimated using Wilke-Chang correlation
(a) EFCE (1978)
(b) Won and Prausnitz (1975)

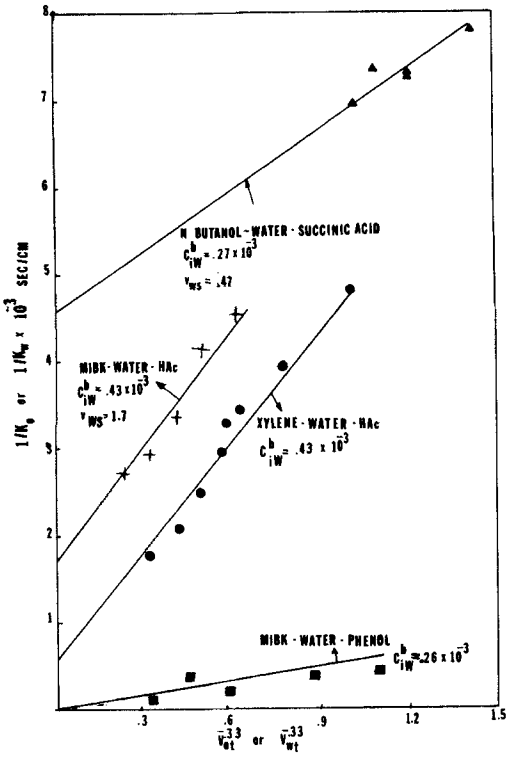

Figure 3. Wilson plot for tube-side flow, hydrophobic MHF modules.

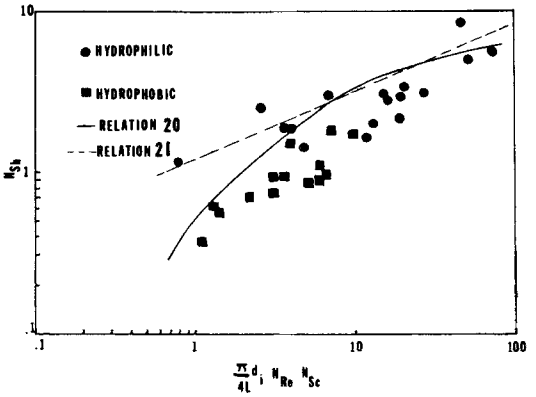

Figure 5. Tube-side N_{Sh} for MHF modules.

determined by the least-square fit of the $\bar{K}$ vs. v data by minimizing an objective function of the form

$$\kappa = \Sigma(1/\bar{K}|_{obs} - 1/\bar{K}|_{calc})^2 \tag{16}$$

This exponent was found to be 0.33 for organic flow on the tube side (for aqueous flow on the tube side for the high-m_i system) and 0.66 for organic flow on the shell side of the extractor (aqueous flow on the shell side for the high-m_i system). As expected from the relations presented earlier, the intercept on the $1/\bar{K}$ axis is 0 for the high-m_i system, is a function of membrane resistance only for a system with $m_i \ll 1$, and is a function of organic phase resistance, membrane resistance, and aqueous phase resistance for $m_i \sim 1$ systems. The intercept is subtracted from the $1/\bar{K}$ values to obtain the tube-side or the shell-side film transfer coefficients for the different systems. The $\bar{k}$ vs. v data thus obtained are plotted in dimensionless form in Figures 5 and 6.

The intercept on the $1/\bar{K}$ axis for an $m_i \ll 1$ system being a function only of the membrane resistance, it is used to calculate the tortuosity of the hydrophobic MHF using Eq. 11. The values

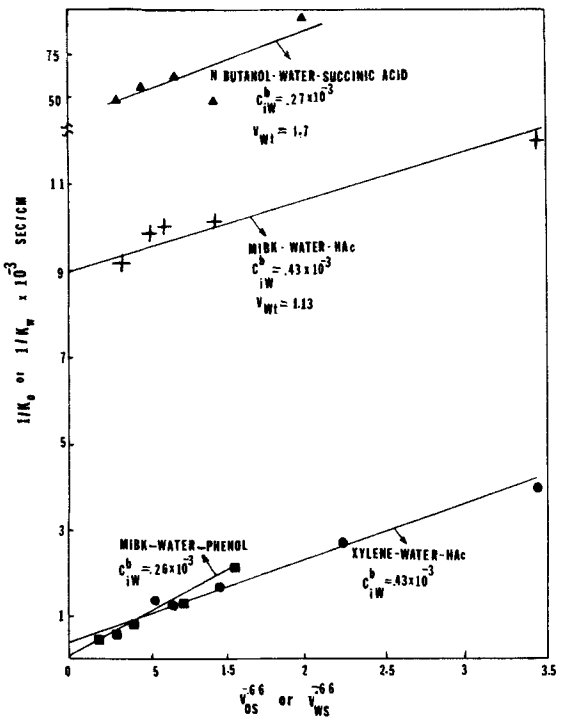

Figure 4. Wilson plot for shell-side flow, hydrophobic MHF modules.

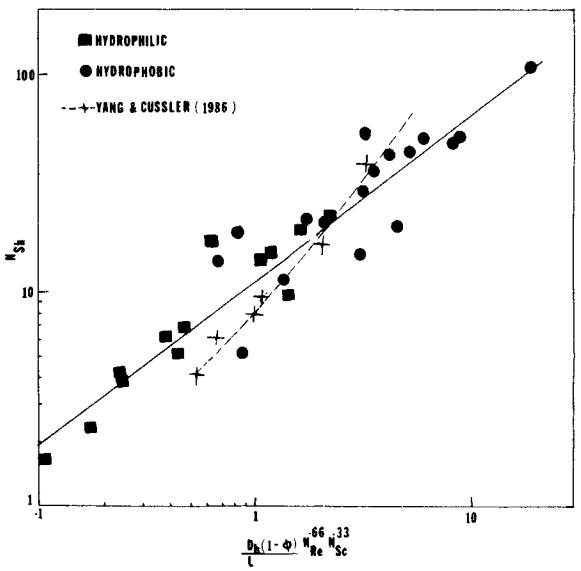

Figure 6. Generalized shell-side N_{Sh} for hydrophilic and hydrophobic extractors.

Table 4. Membrane Mass Transfer Coefficient and Tortuosity for Hollow Fibers

Membrane	System	$k_{mo} \times 10^4$ cm/s	$k_{mw} \times 10^4$ cm/s	τ_M	τ_M (a)
X-20	xylene-water-acetic acid	16.0*		2.4*	—
		15.0†		2.6†	—
X-20	MIBK-water-acetic acid	18.2*		2.8*	2.2
		19.6†		2.6†	(b)
X-20	*n*-Butanol–water–succinic acid	2.08*		2.3*	—
		2.00†		2.4†	—
Cuprophan	MIBK-water-acetic acid	—	7.33*	3.1*	4.2
		—	7.80†	2.9†	—
Cuprophan	*n*-Butanol–water–succinic acid	—	0.717*	13.8*	—
		—	0.706†	14.01†	—
Cuprophan	MBK-water-phenol	—	3.20*	5.6*	—
		—	3.36†	5.4†	—

(a) From gas permeation studies
(b) Bhave and Sirkar (1986a)
*Using tube-side expressions
†Using shell-side expressions

of this membrane resistance and tortuosity are tabulated in Table 4.

For systems of $m_i \simeq 1$, the aqueous-side film transfer coefficients are estimated at the respective flow rates from the correlations developed here, Figures 5 and 6. These estimated values of $\bar{k}_{wt}$ and $\bar{k}_{ws}$ are next substituted in the value of the intercept on the $1/\bar{K}_o$ axis to obtain the membrane resistance k_{mo} of the hydrophobic MHF from Eqs. 9 and 10. These values together with the corresponding tortuosity values of the X-20 membrane are also shown in Table 4.

Hydrophilic MHF

Figures 7 and 8 show the Wilson plots for the hydrophilic MHF extractor no. 2 for organic flow on the tube side (aqueous flow on tube for a system of $m_i \gg 1$) and for organic flow on the shell side (aqueous flow on shell side for a system of $m_i \gg 1$), respectively. The tube- and shell-side film transfer coefficients are obtained as outlined in the theory. These are plotted in dimensionless form in Figures 5 and 6. The membrane resistances are also obtained and, together with the respective membrane tortuosity factors, are shown in Table 4. It is to be noted that the index ν is still 0.33 for organic flow on the tube side and

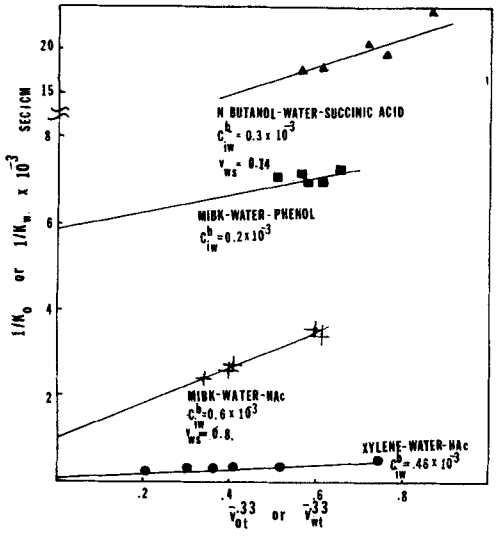

Figure 7. Wilson plot for tube-side flow, hydrophilic MHF modules.

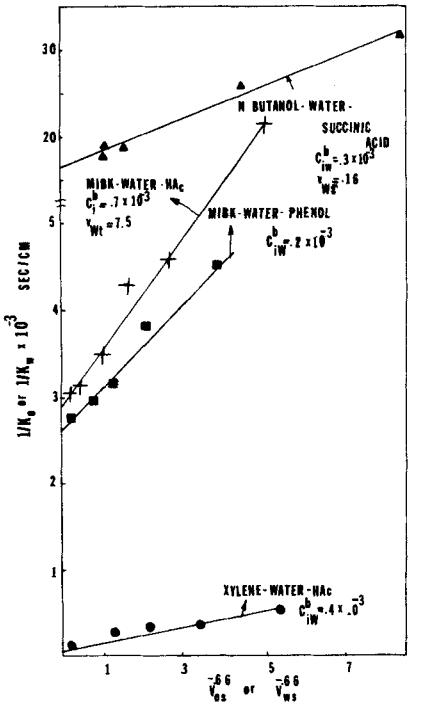

Figure 8. Wilson plot for shell-side flow, hydrophilic MHF modules.

0.66 for organic flow on the shell side. Interestingly, the Wilson plots for the hydrophilic MHF modules are mirror images of the Wilson plots for the hydrophobic MHF modules. This symmetrical behavior of $\bar{K}$ around $m_i \sim 1$ can be predicted quite readily by Eqs. 1–8.

Membrane resistance

The membrane mass transfer coefficients for the various membranes and their tortuosity factors, obtained using Eq. 11, are presented in Table 4. It can be seen that although the k_{mo}'s of the hydrophobic X-20 membrane are very different for the different extraction systems studied, the tortuosity factors are fairly constant and agree very well with those obtained from gas permeation runs. The tortuosity factor of the hydrophilic CUPROPHAN MHF is however not constant and the difference in τ_{Mw} from that determined by gas permeation studies (4.2) requires some explanation.

It has been observed (Farrell and Babb, 1973; Colton et al., 1971) that as the size of the solute molecule approaches the pore size of the CUPROPHAN membrane, the diffusion coefficient of the solute in the liquid filling the pores of the membrane is not the same as its diffusion coefficient for infinite dilution due to hindered diffusion (Beck and Schultz, 1970). A similar effect was observed for flat CUPROPHAN membranes by Prasad and Sirkar (1987b). We believe this explains the drastic increase in the observed tortuosity values of the CUPROPHAN membrane for succinic acid (14.0) and phenol (5.6) systems when compared with the system of a smaller molecule like acetic acid.

It may also be observed from the previous results that the membrane mass transfer resistance is of the same order of magnitude as the other film transfer resistances. Under conditions of extreme m_i (very low or very high), the membrane resistance may become unimportant. For most of the systems, however, the contribution of membrane mass transfer coefficient to the overall resistance cannot be ignored. This is to be contrasted with gas-filled membranes used in gas absorption studies (Yang and Cussler, 1986) where the contribution of membrane resistance to mass transfer can usually be ignored. Further, in such systems only one phase resistance is normally controlling, unlike the situation in liquid-liquid extraction systems studied here.

Pressure drop

Figure 9 shows the pressure drop on the tube and shell sides of the two hydrophilic and the hydrophobic MHF modules as a function of organic velocity for the xylene-water-HAc system. As expected, the pressure drop is higher on the tube side than on the shell side; also, the pressure drop on the tube side of the hydrophilic fiber is higher than that in the hydrophobic MHF. This is due to the smaller diameter of the CUPROPHAN MHF. For larger diameter hollow fibers, pressure drop will be still lower. Additional pressure drop may occur if the shell-side pressure is higher than the tube-side pressure, leading to compressive deformation of the fibers.

Pressure drop in this type of extraction system, however, has to be monitored to maintain the appropriate phase pressure difference everywhere along the extractor. Kim (1984) could not carry out solvent extraction without dispersion as the phase pressure conditions were reversed at the two ends of the module he used. Cooney and Jin (1985) also could not carry out dispersion-free extraction with solvent flow on the shell side because they did not maintain proper phase pressures.

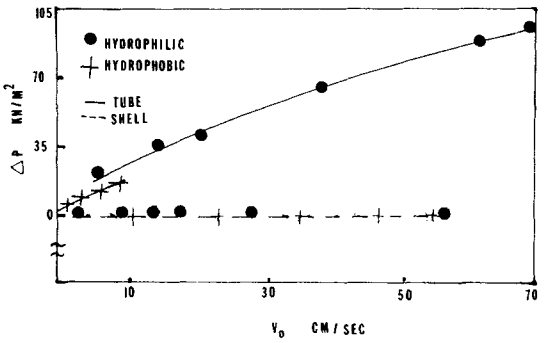

Figure 9. Pressure drop on tube and shell sides for hydrophobic no. 2 and hydrophilic no. 2 extractors.

Generalized film transfer correlations for the hollow-fiber modules

Generalized correlations for N_{Sh} developed in this study for the tube-side flow as well as shell-side flow are presented here. These correlations are valid for $300 < N_{Sc} < 1{,}000$. The correlations are valid for the tube side for $0 < N_{Re} < 60$, and for $0 < N_{Re} < 500$ for flow on the shell side.

Shell Side. The film transfer coefficients for the shell-side flow were calculated as outlined above for both the hydrophobic and the hydrophilic MHF modules. These mass transfer coefficients were next used to calculate the Sherwood number N_{Sh} for the shell side on the basis of a hydraulic diameter D_h defined as:

$$\text{Hydraulic dia.} = 4 \times \text{cross-sectional area of flow/wetted perimeter} \quad (17)$$

This same hydraulic diameter was also used to calculate a Reynolds number, N_{Re}, for flow on the shell side. Since various solvent extraction systems have been used in this study, the Schmidt number, N_{Sc}, is also necessary to obtain correlations for the dimensionless mass transfer coefficient on the shell side.

The exponent of N_{Re} needed to correlate N_{Sh} variation is the same as the exponent ν obtained earlier for organic flow on the shell side (aqueous flow on the shell side for $m_i \gg 1$ system). The N_{Sh} variation with N_{Sc} can be determined as the value of N_{Sh} is available at different N_{Sc}. This exponent was found to be 0.33 by the least-squares fit method. A plot of N_{Sh} against $N_{Re}^{0.6}N_{Sc}^{0.33}$ will then be a straight line. The constant of proportionality α defined by the ratio of N_{Sh} to $N_{Re}^{0.6}N_{Sc}^{0.33}$ will be a function of (among others) the hydraulic radius, the length of the module, and the packing fraction ϕ of the fibers in the modules (this packing fraction will be a function of the diameter-to-pitch ratio usually employed in heat exchanger analysis). One such relation is

$$\alpha = \beta[D_h(1 - \phi)/L] \quad (18)$$

so that

$$N_{Sh} = \beta[D_h(1 - \phi)/L]N_{Re}^{0.6}N_{Sc}^{0.33} \quad (18a)$$

The value of β is found to be 5.8 for the hydrophobic module and 6.1 for the hydrophilic MHF module. Thus, β may be a true constant for both modules.

If a relation such as Eq. 18a is valid, then the plot of N_{Sh}

against $D_h(1-\phi)\,N_{Re}^{0.6}N_{Sc}^{0.33}/L$ should in fact be a straight line common for both modules. This appears to be the case, Figure 6. The slope of this line is then $\beta(5.85)$. Additional studies will have to be done with different modules having different lengths and packing fractions before the above observations can be assumed to be generally valid for MHF extraction modules.

This relation obtained experimentally for mass transfer on the shell side can be compared with the results of heat exchanger studies done with shell-and-tube heat exchangers. Knudsen and Katz (1958) report a value of 0.5 for the exponent of N_{Re} for laminar flow on the shell side of a heat exchanger and a value of 0.6 for turbulent flow on the shell side. Knudsen and Katz also provide a correlation of the form

$$N_{Nu} = 0.002N_{Re}^{0.6}N_{Pr}^{0.33} \tag{19}$$

for heat transfer coefficient on the shell side of a shell-and-tube heat exchanger having secondary flow in the shell.

From gas absorption studies using microporous hollow fibers, Yang and Cussler (1986) have also suggested that flow on the shell side of a hydrophobic hollow-fiber module may be laminar in nature with possible backmixing. They have developed correlations for shell-side N_{Sh} that are functions of the shell packing fractions. Their correlation for fiber bundles having $\phi = 0.25$ and 0.26 is plotted in Figure 6 for comparison with the data obtained in this study.

Studies by Kang et al. (1987) on O_2 transport to water flowing on the shell side of a microporous CELGARD hydrophobic X-20 hollow-fiber bioreactor indicate that the above shell-side relation, Eq. 18a, is quite valid for gas-liquid systems. They have also found that Eq. 18a predicts shell-side mass transfer coefficients to within 10%, whereas the relation developed by Yang and Cussler (1986) was lower by around 50%. Note that the fibers in Kang et al. were 128 cm long, unlike in present study or in Yang and Cussler; the value of ϕ in Kang et al. was also quite low (0.03).

Tube Side. The film coefficients for the flow on the tube side of the hollow fibers were also obtained by the methods outlined previously. Once again, the dependence of N_{Sh} on N_{Re} will be the same as that of $\bar{K}_o$ on v_{or}. The index, ν, of this correlation has a value of 0.33. It was also found that N_{Sh} varied with N_{Sc} to the power of 0.33.

The dimensionless film coefficients for the tube side are shown in Figure 5. It is to be noted that these film transfer coefficients are based on a logarithmic mean driving force ΔC_{lm}. It was found that in the inlet and outlet concentration ranges used here, the logarithmic mean driving force and the arithmetic mean driving force were very close to each other.

The solid line in Figure 5 is the theoretically obtained series solution of the Graetz problem with constant wall concentration, fully developed parabolic velocity profile, and developing concentration profile (Skelland, 1974a). This is mathematically represented as

$$N_{Sh} = 0.5(d_i/L)N_{Re}N_{Sc}\theta \tag{20}$$

where

$$\theta = \frac{1 - \sum_{n=1}^{\infty}\{-4(B_n/\beta_n)(d\phi/dr_+)_{r_+=1}\exp[(-\beta_n^2 L/r_i/N_{Re}N_{Sc})]\}}{1 + \sum_{n=1}^{\infty}\{-4(B_n/\beta_n)(d\phi/dr_+)_{r_+=1}\exp[(-\beta_n^2 L/r_i/N_{Re}N_{Sc})]\}} \tag{20a}$$

The concentration profile on the tube side was not fully developed. This is to be expected as the L/d_i of the two modules used here are not very high (hydrophobic MHF modules no. 2, no. 3 = 800, hydrophilic MHF module no. 2 = 400). It is also to be noted that the theoretical expression is based on arithmetic average driving force rather than on logarithmic mean driving force for the concentration difference.

The above series solution, Eq. 20, converges to the more compact form of the Leveque solution at $N_{Gz}(N_{Gz} = \pi d_i N_{Re}N_{Sc}/4L)$ over 400 (Skelland, 1974b):

$$N_{Sh} = 1.62[(d_i/L)N_{Re}N_{Sc}]^{0.33} \tag{21}$$

It can be seen that for a first order of approximation, the flow in the lumen side can be viewed as laminar. Solutions obtained by Leveque and the Seider-Tate correlation can at best be viewed as a rough estimate of the actual conditions existing on the lumen side of the contactor. In all the experiments done here, N_{Gz} never exceeded 100. For higher N_{Gz}, low values of L and high values of velocity are needed.

The differences in the theoretical and the experimentally observed N_{Sh} can be due to several causes. First the boundary condition of constant wall concentration is not strictly valid, especially where a significant amount of solute is extracted. Second, the hollow fibers deform under excess external pressure conditions (high pressure on the shell side). This leads to a reduction of tube-side flow area and will lead to inaccuracies in the determination of the tube side N_{Re} and N_{Sh}. This is especially true for the hydrophilic MHF's used here since they are highly swollen and hence are not very rigid. It has been observed (Frank, 1986) that Newman's extension of the Leveque solution with only the first term fits almost perfectly the mass transfer data obtained in single microporous hydrophobic hollow-fiber studies with not very long fibers. The problem then seems to lie in the fiber bundle itself. Recent studies with hollow-fiber dialyzers have shown that there are maldistributions of flow in a hollow-fiber bundle depending on the inlet and outlet header design (Park and Chang, 1986). Obviously, additional studies will have to be conducted before firmer conclusions can be drawn.

Discussion

The results presented earlier clearly show that dispersion-free solvent extraction can be carried out efficiently using either hydrophilic or hydrophobic MHF's. A few obvious issues of interest are the advantages of MHF modules over conventional dispersion-based contactors for extraction and the advantages (or disadvantages) of hydrophobic over hydrophilic hollow-fiber membranes.

Membrane-based solvent extraction introduces an added resistance of the membrane phase to the interphase mass transfer. Overall mass transfer coefficients obtained in a membrane extractor are therefore likely to be lower for comparable values of phase transfer coefficients. This is to be balanced against extremely high interfacial area per unit volume available in a membrane contactor. Additionally, since there is no flooding, the phase transfer coefficients can have high values if the phase velocities are high.

Conventional packed-bed analysis (Treybal, 1963) utilizes an HTU and NTU concept where HTU will determine the effi-

Table 5. HTU for Hollow-Fiber Modules as a Function of m_i

	Module								
	Hydrophobic No. 2 $a = 27.2\ cm^{-1}, \phi \sim 0.2$			Hydrophobic No. 3 $a = 46.8\ cm^{-1}, \phi = 0.4$			Hydrophilic No. 2 $a = 17.36\ cm^{-1}, \phi \sim 0.09$		
m_i	Q_{or} cm^3/s	$K_o a \times 10^3$ s^{-1}	HTU m	Q_{or} cm^3/s	$K_o a \times 10^3$ s^{-1}	HTU m	Q_{or} cm^3/s	$K_o a \times 10^3$ s^{-1}	HTU m
0.013	0.14	10.8	0.79	—	—	—	0.64	173	0.227
0.52	0.12	5.76	1.26	—	—	—	0.1	3.49	1.74
1.5	0.02	0.56	2.17	—	—	—	0.015	0.56	1.63
50*	0.08	11.6	0.42	—	—	—	0.06	3.2	1.12
50*	—	—	—	0.18	51.6	0.21	—	—	—

*Values are for Q_{aq} and $K_w a$

ciency of the contactor. The HTU is defined as

$$\text{HTU} = Q_{or}/(\overline{K}_o a \times \text{empty shell cross-sectional area}) \quad (22a)$$

or

$$\text{HTU} = Q_{aq}/(\overline{K}_w a \times \text{empty shell cross-sectional area}) \quad (22b)$$

High values of HTU will show poorly contacted phases. Table 5 shows some of the values of HTU's obtained in this study. The listed values of HTU's are in the lowest range of values reported (Treybal, 1963). These values were calculated based on the actual interfacial area per unit volume a available in this work. Commercial hollow-fiber units used in reverse osmosis and dialysis have much higher a's and hence the HTU's possible with commercial modules will still be lower. Note further that these HTU's are independent of the interfacial tension of the system, unlike conventional contactors.

The next important question is the selection of membranes. Figure 10 shows the overall mass transfer coefficients of the two hydrophobic and hydrophilic MHF's under identical conditions of v_{or} and v_{aq}. It can be seen that for a very low m_i system the overall mass transfer coefficient is higher for a hydrophilic MHF than for a hydrophobic MHF, while at high values of m_i the situation is reversed. This symmetric behavior around $m_i = 1$ is quite readily predicted from the equations for the overall mass transfer coefficient.

A systematic design of hollow-fiber-based, dispersion-free solvent extraction technique will involve estimation of all the individual mass transfer coefficients: tube-side, shell-side, and membrane resistances. Under limiting conditions of m_i, one or the other film transfer coefficient may control the overall mass

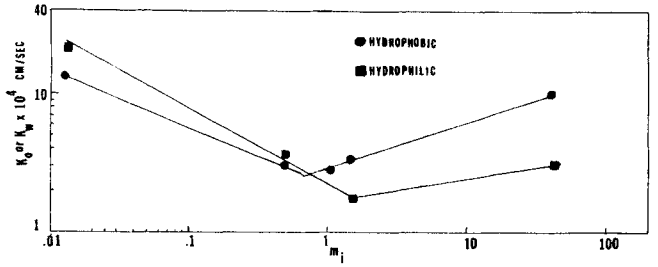

Figure 10. Overall mass transfer coefficients as functions of m_i.
$(N_{Re})_{tube} = 50$; $(N_{Re})_{shell} = 360$

transfer of a solute. However, membrane mass transfer resistance cannot be ignored in general.

Often a solute is extracted (or back-extracted) into an aqueous phase from an organic phase. The governing relations described here between the overall $\overline{K}$ and the individual $\overline{k}$'s can still be used since they are unaffected by the direction of transport (Treybal, 1963; Alexander and Callahan, 1985).

This dispersion-free technique has now been investigated in our laboratory with a variety of extraction systems; these include di-butyl pthalate–water–ethanol and *n*-methyl pyrrolidone–*n*-heptane–toluene, in addition to the systems presented here. A number of other systems currently under investigation do not also display any operational problems. Dispersion-free metal extraction has also been studied (Alexander and Callahan, 1987). Systems with chemical reactions have been investigated by others (Stanley and Quinn, 1987).

Ultrafiltration (UF) membranes can be used for solvent extraction; however, one has to be cautious as these membranes are designed for specific molecular weight cutoff and therefore may prevent larger solute species from being extracted. This is going to be a potential problem in the biochemical industry were biopolymer separations (protein extraction) are being increasingly explored. Care must be taken to ensure selection of a membrane for each extraction system such that hindered diffusion is not important or else the rate of extraction will be drastically reduced.

The low porosity of UF membranes will increase the membrane resistance considerably. A large thickness of porous backing in asymmetric UF membranes will similarly increase membrane resistance during solvent extraction. Additional considerations are needed about the breakthrough pressure *vis-a-vis* the membrane pore size. Since UF membranes are asymmetric, only the pore dimensions at the location of the phase interface will be relevant.

The important issue of the economic viability of this form of contacting has not been considered here. A detailed economic analysis of the proposed method of dispersion-free contacting will be necessary to take it beyond the laboratory stage. We understand that such scale-up studies are already going on.

Conclusions

This work provides extensive data to develop a first-order mass transfer characterization of dispersion-free solvent extraction with microporous hollow-fiber modules. Using the correct phase pressure difference ensures dispersion-free operation whether the membrane is hydrophobic or hydrophilic. Unhin-

dered diffusion through tortuous membrane capillaries describes satisfactorily the membrane transfer coefficient unless the membrane pore sizes are low and solute dimensions are large enough to cause hindered diffusion. The Graetz solution for constant wall concentration describes the lumen-side mass transfer coefficient more satisfactorily than the Leveque solution. A correlation for the shell-side Sherwood number having an $N_{Re}^{0.6} N_{Sc}^{0.33}$ dependence provides a resonable description of the data.

The HTU values achieved with such membrane contactors are low and are comparable to the lowest reported for conventional extractors. The membrane resistance is generally quite significant unless the solute distribution coefficient m_i has extreme values. For comparable boundary layer coefficients and membrane pore sizes and statistics, hydrophobic membranes are to be preferred for $m_i > 1$ systems, whereas hydrophilic membranes are preferable for $m_i < 1$ systems.

Acknowledgment

The microporous hollow fibers used in this study were provided by Celanese Separations Products, Charlotte, NC and ENKA Corporation, FRG. We wish to acknowledge experimental help provided by R. Basu. Summer support for R. Prasad by the Filtration Society, New York chapter, is gratefully acknowledged.

Notation

a = area per unit volume of hollow-fiber modules, cm^{-1}
C_{iw}^b = concentration of solute species in aqueous phase, mol/cm^3
C_{io}^b = bulk concentration of i in organic phase, mol/cm^3
d_i = inner diameter of a hollow fiber, cm
d_o = outer diameter of a hollow fiber, cm
d_{lm} = log mean diameter of a hollow fiber, cm
D_h = hydraulic diameter of the shell side of MHF module, cm
D_{io}, D_{iw} = diffusion coefficient of i in organic, aqueous phase, cm^2/s
k_{mo}, k_{mw} = membrane transfer coefficient for hydrophobic, hydrophilic membrane, cm/s
k_{os}, k_{ot} = organic phase film transfer coefficient for organic flow on shell side, tube side of a hollow-fiber module, cm/s
k_{ws}, k_{wt} = aqueous phase film transfer coefficient for aqueous flow on shell side, tube side of a hollow-fiber module, cm/s
K_o, K_w = overall mass transfer coefficient based on organic phase, aqueous phase, cm/s
L = length of MHF module, cm
m_i = solute distribution coefficient between organic and aqueous phases, C_{io}/C_{iw}
N_{Gz} = Graetz number, $\pi d_i N_{Re} N_{Sc}/4L$
N_{Re} = Reynolds number, $d_i v/\eta$ or $D_h v/\eta$
N_{Sc} = Schmidt number, η/D_i
N_{Sh} = Sherwood number, $\bar{K}d_i/D_i$, $\bar{K}D_h/D_i$
Q_{aq} = aqueous flow rate, cm^3/s
Q_{or} = organic flow rate, cm^3/s
r_i = inner radius of hollow fiber, cm
r = radial location in a hollow fiber, cm
r_+ = r/r_i
v_{or}, v_{aq} = velocity of organic, aqueous phases, cm/s
v_{os}, v_{ot} = velocity of organic phase on shell side, tube side of a hollow-fiber module, cm/s
v_{ws}, v_{wt} = velocity of aqueous phase on shell side, tube side of a hollow-fiber module, cm/s

Greek letters

ϕ = packing fraction of shell side of MHF modules
ϵ_M = porosity of membrane
τ_M = tortuosity of membrane
ν_s, ν_t = index for correlating N_{Sh} to N_{Re}
η = kinematic viscosity, cm^2/s

Subscripts and superscripts

M = membrane phase
o = organic phase
w = aqueous phase
$-$ = module-averaged quantities

Literature Cited

Alexander, P. R., and R. W. Callahan, "Liquid-Liquid Extraction and Stripping of Gold with Microporous Hollow Fibers," manuscript (1987).

Beck, R. E., and J. S. Schultz, "Hindered Diffusion in Microporous Membranes with Known Pore Geometry," *Science*, **170**, 1302 (1970).

Bhave, R. R., and K. K. Sirkar, "Gas Permeation and Separation with Aqueous Membrane Immobilized in Microporous Hydrophobic Supports," Paper no. 246, *8th Am. Chem. Soc. Rocky Mountain Regional Meet.*, Denver (June, 1986); see also *Am. Chem. Soc. Symp. Ser.*, **347**, "Liquid Membranes: Theory and Applications," Ch. 10, 1987 (1986a).

———, "Gas Permeation and Separation by Aqueous Membranes Immobilized Across or in a Thin Section of Hydrophobic Microporous CELGARD Films," *J. Mem. Sci.*, **27**, 41 (1986b).

Colton, C. K., K. A. Smith, E. W. Merrill, and P. C. Farrell, "Permeability Studies with Cellulosic Membranes," *J. Biomed. Mater. Res.*, **5**, 459 (1971).

Cooney, D. O., and Chi-Lem Jin, "Solvent Extraction of Phenol from Aqueous Solution in a Hollow-Fiber Device," *Chem. Eng. Commun.*, **37**, 173 (1985).

Dahuron, L., and E. L. Cussler, "Protein Extraction with Hollow Fibers," *AIChE J.*, **34**(1), 130 (1988).

EFCE (European Federation of Chemical Engineers) Working Party on Distillation, Absorption, and Extraction, *Recommended Systems for Liquid Extraction Studies*, T. Misek, ed., Inst. Chem. Engineers, Rugby, UK (1978).

Farrell, P. C., and A. L. Babb, "Estimation of Permeability of Cellulosic Membranes from Solute Dimensions and Diffusivities," *J. Biomed. Mater. Res.*, **7**, 275 (1973).

Frank, G. T., "Membrane Solvent Extraction with Hydrophobic Microporous Hollow Fibers and Extractive Bioreactor Development for Fuel Ethanol Production," Ph.D. Thesis, Stevens Inst. Technol., Hoboken, NJ (1986).

Frank, G. T., and K. K. Sirkar, "Alcohol Production by Yeast Fermentation and Membrane Extraction," *Biotechnol. Bioeng. Symp. Ser.*, **15**, 621 (1985).

———, "An Integrated Bioreactor-Separator: *In situ* Recovery of Fermentation Products by a Novel Dispersion-free Solvent Extraction Technique," *Biotechnol. Bioeng. Symp. Ser.*, **17**, 303 (1986).

Kang, W., R. Shukla, G. T. Frank, and K. K. Sirkar, "Oxygen Transport and Product Removal in a Locally Integrated Tubular Hollow-Fiber Bioreactor," *9th Symp. Biotechnol. for Fuels, Chemicals*, Boulder, CO (May 1987).

Kiani, A., R. R. Bhave, and K. K. Sirkar, "Solvent Extraction with Immobilized Interfaces in a Microporous Hydrophobic Membrane," *J. Mem. Sci.*, **20**, 125 (1984).

Kim, B. M., "Membrane-Based Extraction for Selective Removal and Recovery of Metals," *J. Mem. Sci.*, **21**, (1984).

Knudsen, J. G., and D. L. Katz, *Fluid Dynamics and Heat Transfer*, McGraw-Hill, New York (1958).

Malm, C. J., L. B. Genung, and J. V. Fleckstein, "Densities of Cellulosic Esters," *Ind. Eng. Chem.*, **39**, 1499 (1947).

Park, J. K., and H. N. Chang, "Flow Distribution in the Lumen Side of a Hollow-Fiber Module," *AIChE J.*, **32**, 1937 (1986).

Prasad, R., "Dispersion-Free Solvent Extraction Through Microporous Membranes," Ph.D. Thesis, Stevens Inst. Technol., Hoboken, NJ (1986).

Prasad, R., and K. K. Sirkar, "Microporous Membrane Solvent Extraction," *Sep. Sci. Tech.*, **22**(2,3), 619 (1987a).

———, "Solvent Extraction with Microporous Hydrophilic and Composite Membranes," *AIChE J.*, **33**(7), 1057 (1987b).

Prasad, R., R. R. Bhave, A. Kiani, and K. K. Sirkar, "Further Studies on Solvent Extraction with Immobilized Interfaces in a Microporous Hydrophobic Membrane," *J Mem. Sci.*, **26**, 79 (1986).

Qi, Zhang, and E. L. Cussler, "Microporous Hollow Fibers for Gas

Absorption; Mass Transfer Across the Membrane," *J. Mem. Sci.*, **23**, 333 (1985).

Radovich, J. M., W. C. Babcock, and K. R. Pearson, "Removal of SO_2 from Flue Gas in a Hollow-Fiber Membrane Contactor," Paper no. 249, *8th Am. Chem. Soc. Rocky Mount. Regional Meet.*, Denver (June, 1986).

Skelland, A. H. P., *Diffusional Mass Transfer*, Wiley, New York, p. 164 (1974a); p. 167 (1974b).

Stanley, T. J., and J. A. Quinn, "Phase Transfer Catalysis in Membrane Reactors," Paper No. 98f, AIChE Meet., Chicago (Nov. 14, 1985).

Treybal, R. E., *Liquid Extraction*, 2nd ed., McGraw-Hill, New York (1963).

Wilson, E. E., "A Basis for Rational Design of Heat Transfer Apparatus," *Trans. ASME*, **37**, 47 (1915).

Won, K. W., and J. M. Prausnitz, "Distribution Coefficient of Phenolic Solutes between Water and Organic Solvents," *J. Chem. Thermody.*, **7**, 661 (1975).

Yang, M. C., and E. L. Cussler, "Designing Hollow-Fiber Contactors," *AIChE J.*, **32**, 1910 (1986).

Manuscript received Apr. 1, 1987, and revision received July 23, 1987.